Vortex crystals from 2D Euler flow: Experiment and simulation

D. A. Schecter, D. H. E. Dubin, K. S. Fine, and C. F. Driscoll
Physics Department, University of California at San Diego, La Jolla, California 92093

Vortex-in-cell simulations that numerically integrate the 2D Euler equations are compared directly to experiments on magnetized electron columns [K. S. Fine, A. C. Cass, W. G. Flynn, and C. F. Driscoll, ''Relaxation of 2D turbulence to vortex crystals,'' Phys. Rev. Lett. **75**, 3277 (1995)], where turbulent flows relax to metastable vortex crystals. A vortex crystal is a lattice of intense small diameter vortices that rotates rigidly in a lower vorticity background. The simulations and experiments relax at the same rates to vortex crystals with similar vorticity distributions. The relaxation is caused by mixing of the background by the intense vortices: the relaxation rate is peaked when the background circulation is 0.2–0.4 times the total circulation. Close quantitative agreement between experiment and simulation provides strong evidence that vortex crystals can be explained without incorporating physics beyond 2D Euler theory, despite small differences between a magnetized electron column and an ideal 2D fluid. © *1999 American Institute of Physics.* [S1070-6631(99)00404-3]

I. INTRODUCTION

The free relaxation of 2D turbulence has been a topic of active research for decades, with applications in astrophysics, geophysics, and plasma physics.[1–4] Experiments and numerical simulations have shown that the relaxation process typically involves the chaotic advection and merger of intense vortices and the production of vorticity filaments that evolve to increasingly fine length scales. In the past, variational principles have been used to predict the final state of the coarse-grained vorticity distribution. In some cases, the final states are seen to maximize entropy functionals,[4,5] but different initial conditions can lead to states of minimum enstrophy.[4,6,7]

Strongly magnetized electron columns have recently been used to study the relaxation of 2D turbulence experimentally. One of the first of these experiments showed that certain hollow vortices relax to minimum enstrophy states after they experience a Kelvin–Helmholtz instability.[7] More recent experiments on electron columns[8] suggest that ideal 2D turbulence can self-organize into states where enstrophy is not globally minimized and entropy is not globally maximized. In these experiments, the chaotic advection of intense vortices ''cools,'' mergers cease and the vortices settle into a lattice that rotates rigidly in a lower vorticity background. These rigid patterns persist for around 10^4 rotation periods before they are finally dissipated by nonideal effects. When the intense vortices have equal strength, the patterns are symmetric, and for this reason they have been called vortex crystals. A selection of vortex crystals is displayed in Fig. 1 (taken directly from Ref. 8).

Although similar vortex crystals have been seen in dissipative systems such as two-fluid liquid helium,[9] the rapid relaxation of a strongly magnetized electron column is believed to closely follow 2D Euler dynamics. It is surprising that inviscid fluid equations should provide a mechanism for cooling the chaotic advection of the intense vortices to a lattice in rigid rotation; to our knowledge, no previous experiment or simulation has demonstrated the spontaneous formation of vortex crystals from freely relaxing nondissipative turbulence. In order to show that the observed relaxation of turbulent flow to vortex crystals can be explained without incorporating physics beyond the ideal 2D fluid model, we compare the experiments directly to vortex-in-cell (VIC) simulations that numerically integrate the 2D Euler equations.[10] The experiments and simulations are shown to relax at the same rates to vortex crystals with similar vorticity distributions. Close agreement between experiment and simulation provides strong evidence that 2D Euler theory alone can explain the formation of vortex crystals.

Of course, any numerical integration of the 2D Euler equations will differ from an exact solution. There is always concern that a new result is an artifact of the particular discretization scheme. However, we have confirmed that the VIC simulations conserve the robust integral invariants of 2D Euler flow. Moreover, the relaxation to a vortex crystal state occurs at the same rate whether the number of point-vortices in a simulation is 8×10^5, 4×10^5, or 1×10^5. In addition, the rate of relaxation does not change when the simulation's grid-point spacing (cell size) is increased by a factor of 2 or 4. Only subtle differences in the final vorticity distribution appear when the simulation parameters are changed. For example, an additional small vortex may appear in the final pattern.

By adding a slight random walk to each point-vortex in our simulation, we can observe the effect of a simple diffusive viscosity on the formation of vortex crystals.[11] Using this technique, we will show explicitly that viscosity in the Navier–Stokes equations acts to counter the formation of vortex crystals rather than enhance the rate at which the system of intense vortices relaxes to a pattern in rigid rotation. The reason is simple; viscosity acts to diffuse the intense vortices and level the vorticity distribution. The very high
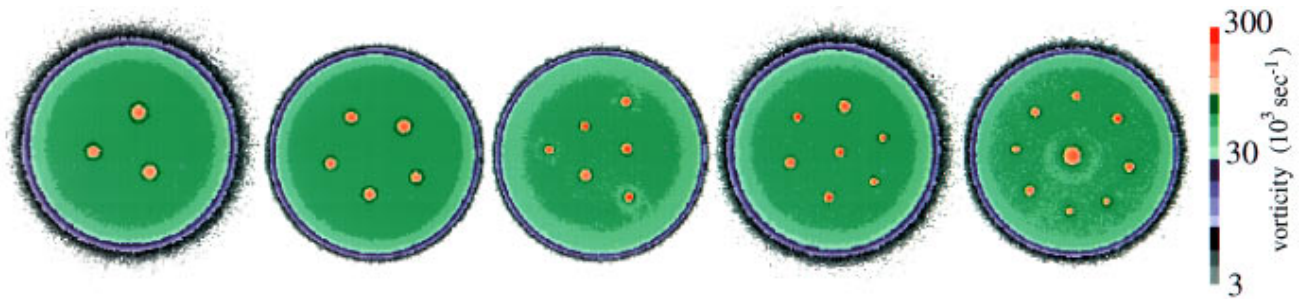
FIG. 1. Vortex crystals observed in magnetized electron columns (Ref. 8). The color map is logarithmic. This figure shows vortex crystals with (from left to right) $M = 3$, 5, 6, 7, and 9 intense vortices immersed in lower vorticity backgrounds. In a vortex crystal equilibrium, the entire vorticity distribution $\zeta(r, \theta)$ is stationary in a rotating frame; i.e., ζ is a function of the variable $-\psi + \frac{1}{2}\Omega r^2$, where ψ is the stream function and Ω is the frequency of the rotating frame.

Reynolds number that is required to see vortex crystals may help explain why the formation of vortex crystals has not been observed in previous experiments or simulations of the Navier–Stokes equations.

As mentioned previously, vortex crystals cannot be explained either by considering global maximum entropy states[5] or minimum enstrophy states.[6] Although complex vorticity patterns consisting of several asymmetric vortices can be predicted on the basis of maximum global entropy theory for certain special initial conditions, these patterns (corresponding to negative temperature states) typically consist of rather large slowly varying vortices that fill the confinement region, not the intense small vortices observed here. Furthermore, it is clear from observations of the evolution that the central regions of intense vorticity in the strong vortices arise from the initial flow, which consists of an intense striated vorticity pattern, and that these central regions remain unmixed with the larger low vorticity background. Global maximum entropy theory, which presumes ergodic mixing of all vorticity elements, clearly does not apply to this flow.

However, maximum entropy theory may apply to part of the flow—the low vorticity background. In a recent Letter,[12] Jin and Dubin hypothesized that the turbulent flow is brought to a vortex crystal equilibrium due to the violent mixing of the diffuse background by the intense vortices. Assuming that the mixing of the background is ergodic, they argued that a vortex crystal is a state that maximizes disorder (entropy) in the background, subject to the constraints of 2D Euler flow. This regional maximum fluid entropy theory (so-called because only the background vorticity is mixed, and the strong vortices are taken to be pointlike without internal degrees of freedom) was shown to accurately predict the final positions of the intense vortices and the final background vorticity distributions of the experiments in Fig. 1, given the number of vortices and the energy, angular momentum, and circulation.

Here, we present further evidence that the system is driven to a vortex crystal equilibrium through the turbulent mixing of the background by the intense vortices. First, we observe that the intense vortices do not cool to a vortex crystal when the background is removed from the simulation. We also find that the intense vortices do not cool in the opposite limit, when the background circulation dominates the circu-

lation of the intense vortices. Presumably, the relaxation rate goes to zero in this limit because the vortices become ineffective mixers. As expected, the relaxation rate peaks at some intermediate level of the background, which is strong enough to influence the intense vortices but weak enough to be mixed.

II. CONCERNS WITH 2D EULER THEORY AND THE NEED TO COMPARE EXPERIMENT TO SIMULATION

A. Experiment

Figure 2 shows the experimental apparatus (Penning–Malmberg trap) with CCD imaging diagnostic. The electrons are confined radially by the Lorentz force of a uniform magnetic field that is applied along the z-axis. They are trapped axially by negative voltages at opposite ends of the confinement cylinder.

The imaging diagnostic destructively measures the z-integrated electron density. By raising one end-potential rapidly to ground, the electrons are dumped onto a phosphor screen that radiates photons in proportion to the number of incident electrons, and the image is recorded with a 512 $\times$ 512 pixel CCD camera. Although the imaging is destructive, variations in the initial conditions are small ($\delta n/n \leqslant 10^{-2}$), so by dumping the electrons at a sequence of times we are able to study flows with this technique.

B. Ideal 2D fluid approximation

We can approximate the $r - \theta$ flow of electron density in our magnetized electron columns with the 2D drift-Poisson equations,[13]
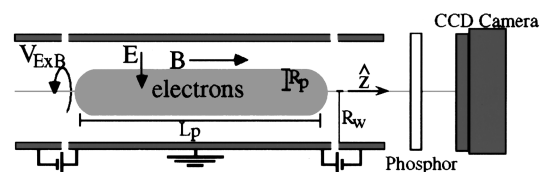

FIG. 2. Cylindrical Penning–Malmberg trap and destructive imaging diagnostic. **E** is the electric field produced by the electrons and **B** is the uniform applied magnetic field. $V_{\mathbf{E}\times\mathbf{B}}$ denotes the counterclockwise **E**$\times$**B** drift of the electrons. $R_w = 3.5$ cm, $R_p \sim 1.5 - 2.5$ cm, and $L_p \sim 50$ cm.

$$\partial n/\partial t + \mathbf{v}\cdot\nabla n = 0, \tag{1a}$$

$$\mathbf{v} = \hat{z}\times c\nabla\phi/B, \tag{1b}$$

$$\nabla^2\phi = 4\pi en. \tag{1c}$$

Here, $n(r,\theta,t)$ is the z-averaged electron density, $\mathbf{v}(r,\theta,t)$ is the $\mathbf{E}\times\mathbf{B}$ drift in the $r-\theta$ plane, and $\phi(r,\theta,t)$ is the electrostatic potential. The equations are 2D because the electron motion has been averaged over a bounce period in the z-direction. The boundary condition at the wall of the confinement cylinder is $\phi(R_w,\theta,t)=0$.

The equations that evolve vorticity, $\zeta\equiv\hat{z}\cdot\nabla\times\mathbf{v}$, can be obtained directly from the drift-Poisson equations. They are the Euler equations,

$$\partial\zeta/\partial t + \mathbf{v}\cdot\nabla\zeta = 0, \tag{2a}$$

$$\mathbf{v} = \hat{z}\times\nabla\psi, \tag{2b}$$

$$\nabla^2\psi = \zeta, \tag{2c}$$

which also govern the flow of 2D inviscid incompressible fluids. The new field ψ is a rescaled electrostatic potential, $\psi\equiv c\phi/B$, and serves as a streamfunction for the flow. Comparing Eqs. (1) and (2), we see that the vorticity is proportional to the electron density by the relation $\zeta=4\pi ecn/B$. So, by measuring the electron density we are also taking a direct measurement of vorticity, insofar as 2D drift-Poisson theory is a good model for the experiment. The condition that ψ equals zero at R_w corresponds to a free-slip boundary condition at the wall of a circular container.

However, there is concern that the approximations used to derive Eqs. (1) and (2) neglect terms that are essential to the formation of vortex crystals. To begin with, Eqs. (1) and (2) describe the experiments only if the time scales associated with electron motion satisfy the inequalities $\tau_c\ll\tau_z\ll\tau_{\mathbf{E}\times\mathbf{B}}$. Here, τ_c denotes the period for an electron's small gyrations around a magnetic field line (its cyclotron motion), τ_z is the time required for an electron to bounce between the ends of the plasma column in the z-direction, and $\tau_{\mathbf{E}\times\mathbf{B}}$ is the time scale for $\mathbf{E}\times\mathbf{B}$ drift. In our experiments, $\tau_c\sim10^{-3}$ μs, $\tau_z\sim2$ μs, and the internal turnover time for a typical vortex is $\tau_{\mathbf{E}\times\mathbf{B}}\sim20$ μs. Although τ_c is much less than τ_z and $\tau_{\mathbf{E}\times\mathbf{B}}$, the condition that $\tau_z\ll\tau_{\mathbf{E}\times\mathbf{B}}$ is only weakly satisfied. In addition to time scale constraints, there are length scale constraints. For example, the drift-Poisson approximation breaks down at length scales that are smaller than the cyclotron radius ($r_c\sim10$ μm). Furthermore, one assumes that the plasma is infinitely long in deriving Eqs. (1) and (2) since all variation in the z-direction is neglected. In reality, $L_p\sim50$ cm and $R_p/L_p\sim0.05$.

A well-studied correction to the infinite-length approximation is that caused by the static electric fields that confine the plasma in the z-direction. These fields modify the bounce-averaged drift that is given by Eq. 1(b), and depending on circumstances this modification can enhance or suppress shear-flow instabilities.[14,15] In general, the modified drift increases with the kinetic energy of the electrons and a spread in electron energy will cause a vorticity profile to smear.[15]

Another correction to ideal fluid theory arises from the finite number N of "point-vortices" in the experiment. Each electron is like a 2D point-vortex after averaging over its z-motion. The Euler equations evolve the ensemble averaged density of a point-vortex gas only in the lowest order mean-field approximation, which neglects fluctuations due to finite N. These fluctuations can be treated with a collision term on the right-hand side of the continuity Eq. 1(a) or 2(a).[16] This collision term is believed to be responsible for the eventual dissipation of vortex crystals that occurs in the experiments. The time scale for a vortex crystal to dissipate (10^3–10^4 rotations) far exceeds the time required for a vortex crystal to form (10–100 rotations). However, the collision term (due to finite N) may be enhanced at small length scales, and it was previously feared responsible for driving the turbulent flow to the metastable vortex crystal equilibrium.

C. Vortex-in-cell simulation

In this paper, we address concerns over the ideal 2D fluid model by comparing the experiment directly to a VIC simulation that numerically integrates the 2D Euler equations.[10] In the simulation, $N\leqslant8\times10^5$ point-vortices are distributed to match the initial vorticity profile of the experiment. The vorticity is interpolated from the point-vortices to a square grid (usually 513×513) on which Poisson's equation is solved with the boundary condition $\psi(R_w,\theta,t)=0$. The interpolation transfers vorticity from each point-vortex to the four nearest grid-points with the method of area weighting.[10] Poisson's equation is solved with a five-point finite difference scheme that employs multigrid relaxation. The velocity field is obtained on the grid by taking the gradient of ψ and is then interpolated back to the particle positions. The particles move forward in time with second-order Adams–Bashforth steps.

In what follows, we will show that the VIC simulations are in good quantitative agreement with the experiments and that the simulation results are not sensitive to large variations in N or in the grid-point spacing. In doing so, we will demonstrate that vortex crystals are not caused by finite length effects, finite cyclotron radius effects, finite N effects or by any dynamics on time scales rapid compared to $\mathbf{E}\times\mathbf{B}$ drift (such as cyclotron motion or axial motion). In other words, although there exist some differences between a magnetized electron column and an ideal 2D fluid, the observed vortex crystals can be explained without incorporating physics beyond 2D Euler theory [Eq. (2)].

III. COMPARISON OF EXPERIMENT TO SIMULATION

A. Integral invariants

Before making a detailed comparison of experiment to simulation, it is important to verify that both conserve the robust integral invariants of 2D Euler flow. The 2D Euler equations with θ-symmetric boundary conditions conserve the energy $H\equiv-\frac{1}{2}\int d\mathbf{r}^2\zeta\psi$, the canonical angular momentum $P_\theta\equiv\int d\mathbf{r}^2 r^2\zeta$, the total circulation $\Gamma_{\text{tot}}\equiv\int d\mathbf{r}^2\zeta$ ($\sim$ number of electrons) and all higher moments of the vorticity distribution $Z_m\equiv(1/m)\int d\mathbf{r}^2\zeta^m$, where $m=2,3,...,\infty$. By con-
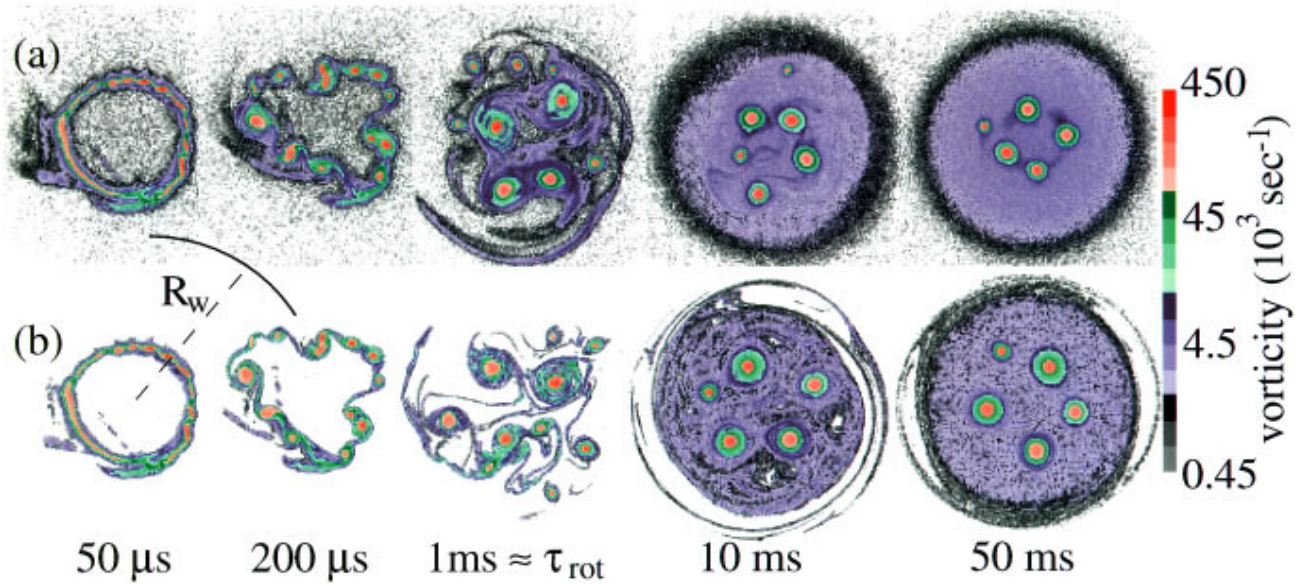
FIG. 3. Sequence I, the formation of a vortex crystal from an annular vorticity distribution: (a) experiment, (b) simulation. The color map is logarithmic and the experimental vorticity is obtained from the relation $\zeta = 4\pi ecn/B$. All vorticity below the shot-noise threshold ($\zeta_{thresh} \sim 2.3 \times 10^3$ s^{-1}) was removed from the simulation's initial condition. The evolution is shown in a reference frame that rotates with frequency 5.872×10^3 rad/s.

struction, our simulations conserve Γ_{tot}. They also conserve energy and angular momentum by roughly one part in 10^3. The experiments show up to 10% declines in Γ_{tot} over the first 100 ms (100–1000 rotations), whereas the normalized quantities H/Γ_{tot}^2 and P_θ/Γ_{tot} fluctuate by only a few percent. The experimental decay in Γ_{tot} over time is probably caused by the slow ionization of background gas, which results in a loss of electrons. Although a small decrease in Γ_{tot} is undesirable, it seems incidental to the formation of vortex crystals. As we will see, the simulations produce vortex crystals while conserving Γ_{tot}.

Although Z_2 and all higher moments of vorticity Z_m are conserved by the 2D Euler equations, their measured values are generally not conserved in freely relaxing 2D turbulence. This is because any physical measurement of vorticity at a given position is an average over a cell of small but finite area. As vorticity filaments stretch and narrow to microscopic length scales, the measured vorticity along the filaments will decrease. An example of this decrease can be observed in Fig. 3, where the low vorticity (blue) regions increase in area over time.

The integrals H, P_θ, and Γ_{tot} are insensitive to measurement coarse-graining of the vorticity. On the other hand, enstrophy Z_2 and all higher moments Z_m are fragile invariants, and their measured values will decrease with time due to coarse-graining.[17] In the experiments, vorticity is coarse-grained on a 512×512 pixel CCD camera, and the measured enstrophy Z_2 typically decays by a factor of 2 during the formation of a vortex crystal. In the VIC simulations, vorticity is coarse-grained on a 513×513 square grid, and the enstrophy of the coarse-grained vorticity also decays by a factor of 2 during the formation of a vortex crystal. We emphasize that a decay in the enstrophy of a coarse-grained vorticity distribution is entirely consistent with the 2D Euler equations.

B. Vortex crystal formation

We now proceed with a detailed comparison of experiment to simulation. Figure 3(a) shows an experiment where an annular vorticity distribution evolves into a vortex crystal. Figure 3(b) shows the results of a VIC simulation that starts with the same annular initial condition. The simulation has $N = 8 \times 10^5$ point-vortices and a 513×513 square grid. We will refer to the flow in Fig. 3 as Sequence I.

In both the experiment and the simulation, a Kelvin–Helmholtz instability generates a "soup" of intense vortices. These vortices chaotically advect, merge and shed filaments that stretch and mix to form a diffuse background. Eventually the chaotic vortex motion cools, mergers stop and in both cases the intense vortices tend to a pattern in rigid rotation. Although our simulation does not reproduce the experiment exactly, both flows produce similar vortex crystals.

Most differences between the experiment and simulation emerge before one rotation period. These differences include the precise shapes and arrangement of intense vortices, and the filamentation which appears to be more "smeared" in the experiment than in the simulation. We speculate that these differences are primarily due to the additional drifts in the experiment that are caused by the electrostatic confinement fields and that vary with the axial kinetic energy of the electrons.[14,15]

Despite subtle differences, the experiment and simulation show good quantitative agreement in several key areas. First, they have similar evolutions in the number M of intense vortices. As in Ref. 8, the vortex census used here is essentially that of McWilliams[18] without the exclusion of elongated vortices; we define an intense vortex as a connected patch of vorticity for which $\zeta > \zeta_{min}$ and for which the mean diameter $d > d_{min}$. Here ζ_{min} and d_{min} are parameters of the counting algorithm. These parameters were changed

Phys. Fluids, Vol. 11, No. 4, April 1999
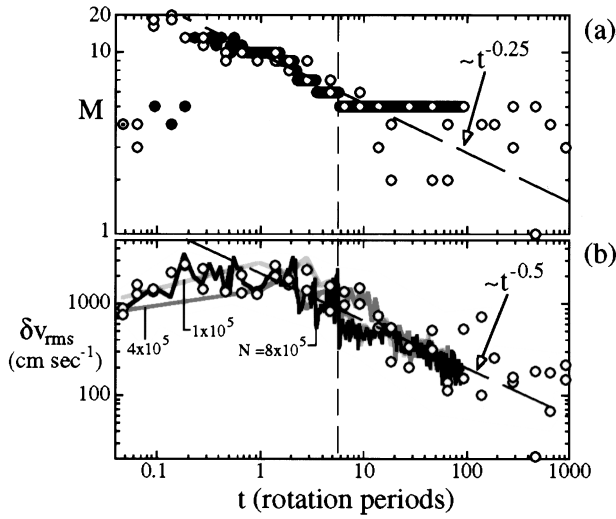
Schecter *et al.*   909

FIG. 4. (a) Number of vortices M vs time for Sequence I. (b) Cooling curves $\delta v_{\mathrm{rms}}(t)$ for same flow. Black, dark grey, and light grey correspond to simulations with $N=8\times10^5$, 4×10^5, and 1×10^5, respectively. Open circles correspond to the experiment. The vertical dashed line indicates the time at which M reaches its terminal value. The slanted dashed lines suggest power-law decays. Time t is normalized to the rotation period of the vortex crystal in the simulation [Fig. 3(b)], $\tau_{\mathrm{rot}}=1.07$ ms.

slightly from those used in Ref. 8, so that vortices smaller than $d_{\mathrm{min}}\equiv0.05$ cm in diameter were not counted. A brief discussion of the uncertainties inherent in this census method can be found at the end of this section.

Figure 4(a) shows that the evolution of the number M of intense vortices in the simulation (solid circles) falls within the scatter of the experimental data (open circles). The high degree of scatter at late times in the experiment is a consequence of slight differences in the initial conditions associated with each experimental ''shot.'' Recall that each experimental datum is taken from a separate evolution due to the destructive imaging technique. After the Kelvin–Helmholtz instability and before M reaches its final value, the evolution in the number of intense vortices resembles a power-law decay, $M\sim t^{-\xi}$ for $0.3<t/\tau_{\mathrm{rot}}<6$. Here $\tau_{\mathrm{rot}}=1.07$ ms is the time averaged rotation period of the vortex crystal in the simulation [Fig. 3(b)]. Linear least-squares fits to log–log plots of the data give $\xi_{\mathrm{sim}}=0.3\pm0.1$ and $\xi_{\mathrm{exp}}=0.2\pm0.1$. Power-law decays in M have been observed in previous simulations of ideal 2D fluid equations[18] and in simulations on discrete vortices that follow punctuated Hamiltonian dynamics.[19] Power law decays occur in many processes where the decay rates $\dot c/c$ are proportional to powers of the concentration c, such as colloidal aggregation, certain chemical reactions and two or three body recombination.[18,20]

During the formation of vortex crystals, the chaotic advection of the intense vortices slowly relaxes, and as mergers stop the intense vortices tend to a pattern that rotates rigidly in a lower vorticity background. We refer to this process as vortex cooling. Vortex cooling is observed to occur at the same rate in the experiment and simulation. To show this requires a quantitative measure of vortex cooling. First, the positions $\{\mathbf{r}_i\}$ $(i=1,2,...,M)$ and the velocities $\{\mathbf{v}_i\}$ of the intense vortices are calculated relative to the flow's center of

vorticity, $\mathbf{r}_i\equiv\int_{A_i}d\mathbf{r}^2(\zeta-\zeta_{\mathrm{min}})(\mathbf{r}-\mathbf{r}_{\mathrm{cv}})/\int_{A_i}d\mathbf{r}^2(\zeta-\zeta_{\mathrm{min}})$ and $\mathbf{v}_i\equiv\int_{A_i}d\mathbf{r}^2(\zeta-\zeta_{\mathrm{min}})(\mathbf{v}-\dot{\mathbf{r}}_{\mathrm{cv}})/\int_{A_i}d\mathbf{r}^2(\zeta-\zeta_{\mathrm{min}})$. Here, A_i denotes the region occupied by the ith intense vortex and $\mathbf{r}_{\mathrm{cv}}$ is the flow's center of vorticity defined by the equation $\mathbf{r}_{\mathrm{cv}}\equiv(1/\Gamma_{\mathrm{tot}})\int d\mathbf{r}^2\mathbf{r}\zeta$. The mean rotation of the intense vortices about $\mathbf{r}_{\mathrm{cv}}$ is then subtracted from each $\mathbf{v}_i$, giving a set of velocity fluctuations $\{\delta\mathbf{v}_i\}$ about the mean rotation, $\delta\mathbf{v}_i\equiv\mathbf{v}_i-r_i\bar\Omega(t)\hat\theta$, where $\bar\Omega(t)\equiv\Sigma_{i=1}^M v_{i,\theta}/\Sigma_{i=1}^M r_i$ (radial-weighted averaging). A discussion of the error in the measurement of $\delta\mathbf{v}_i$ can be found at the end of this section.

As the pattern of intense vortices approaches uniform rotation, the root-mean-square value of the velocity fluctuations tends to zero, i.e., $\delta v_{\mathrm{rms}}\equiv(\Sigma_{i=1}^M\delta\mathbf{v}_i^2/M)^{1/2}\to0$ as $t\to\infty$. We will refer to the graph of δv_{rms} vs time as the cooling curve of the flow.

Figure 4(b) shows the cooling curves for the experiment and for the simulation of Sequence I. The cooling curves are approximately the same. Although one decade of vortex cooling does not suffice to accurately determine the functional form of $\delta v_{\mathrm{rms}}(t)$, a power-law gives a good description at late times, $\delta v_{\mathrm{rms}}\sim t^{-\alpha}$. Linear least-squares fits to log–log plots of the data give $\alpha_{\mathrm{sim}}=\alpha_{\mathrm{exp}}=0.5\pm0.2$ for times greater than one rotation period.

A similar comparison to simulation has been made for an experiment that was taken directly from Ref. 8. We will refer to this flow as Sequence II. Here, the vorticity in the experiment starts as a tightly wound filament, as seen in Fig. 5. Using $N=8\times10^5$ point-vortices and a 513×513 square grid, our simulation failed to produce a vortex crystal from this initial condition. As reported in Ref. 8, small-scale details appear crucial in determining whether the spiral distribution will evolve into a vortex crystal or into an axisymmetric equilibrium. The essential details may have been lost due to the finite resolution of the CCD imaging. Otherwise, the simulation's failure to produce a vortex crystal can only be blamed on slight dynamical differences with the experiment. To compensate, we began the simulation at a later stage of the flow (~4 rotations), at which time there were multiple intense vortices ($M=15$).

Figure 6(a) shows the evolution in the number of intense vortices over time for the simulation (solid black circles) and the experiment (open circles). The grey data will be discussed shortly. The decay rates are similar, but the final number of intense vortices in the simulation ($M=5$) falls below the experimental average ($M\approx7$). Note that in the simulation the last merger event occurs at 25 rotation periods. The final drop in M from 6 to 5 (at $t/\tau_{\mathrm{rot}}\approx450$) corresponds to a small vortex being sheared apart as it periodically passes regions of intense shear-flow produced by neighboring strong vortices.

The cooling curves for the simulation and the experiment are shown in Fig. 6(b). These cooling curves show close agreement during the initial turbulent phase of the flow, when mergers of intense vortices occur regularly. During this time period, least-squares fits to the data give cooling exponents $\alpha_{\mathrm{sim}}=0.5\pm0.2$ and $\alpha_{\mathrm{exp}}=0.4\pm0.1$. However, the cooling curve in the simulation levels off before cooling stops in the experiment. We can resolve this discrepancy in
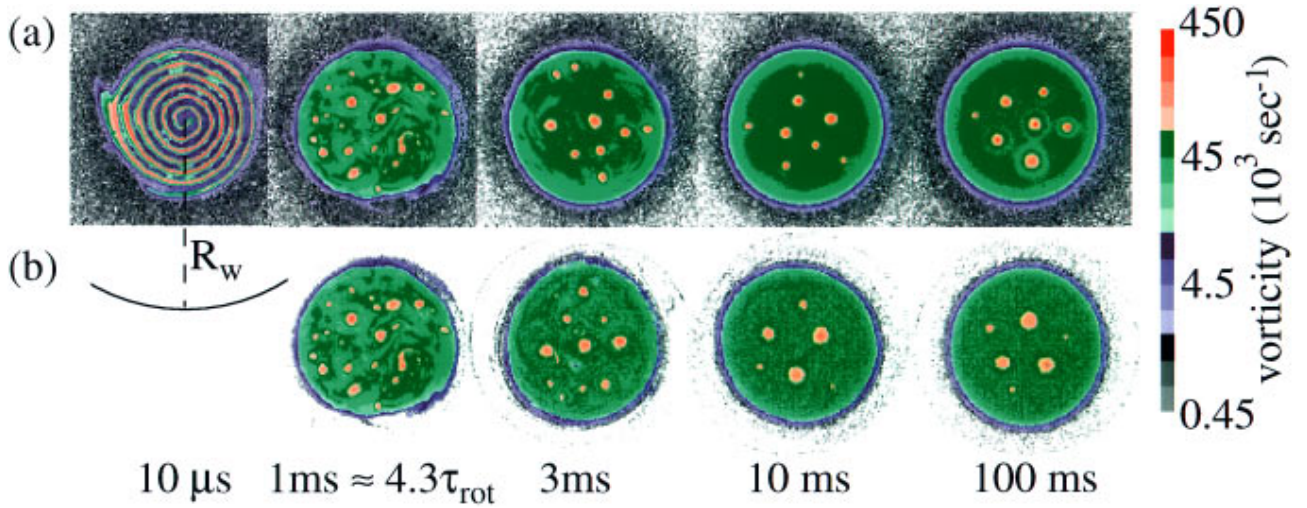
FIG. 5. Sequence II, the formation of a vortex crystal from a spiral vorticity distribution: (a) experiment, (b) simulation. All vorticity below the shot-noise threshold ($\zeta_{thresh} \sim 2.3 \times 10^3$ s^{-1}) was removed from the simulation's initial condition. The evolution is shown in the laboratory frame.

part by observing that in both cases cooling appears to stop shortly after the last merger event. Beyond the last merger, least squares fits to the data give cooling exponents $\alpha_{sim} = 0.0 \pm 0.1$ and $\alpha_{exp} = 0.1 \pm 0.1$.

An additional simulation was initialized to include the measured background vorticity below the shot-noise threshold (the grey fuzz in the experimental images). The data for this simulation are shown in grey in Figs. 6(a) and 6(b). This flow differs from the previous simulation (black) in that the final merger event occurs at a much later time, a time that appears to be more consistent with the experiment (open circles). In addition, the cooling curve levels off at a lower value of δv_{rms}. This enhanced cooling may result from the
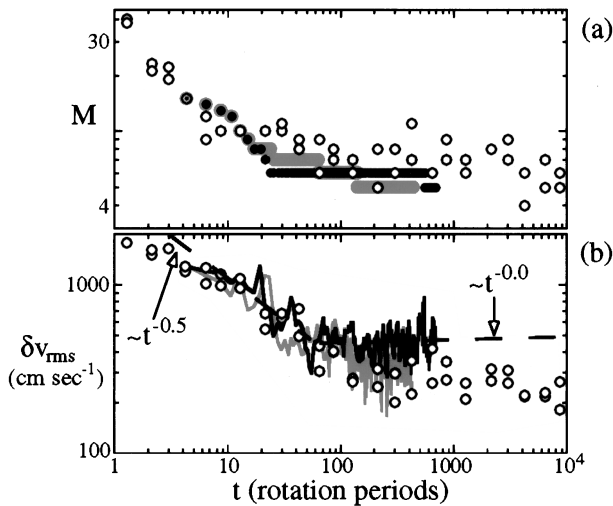

FIG. 6. (a) Number of vortices M vs time for Sequence II. (b) Cooling curves $\delta v_{rms}(t)$ for the same sequence. Black corresponds to the simulation in Fig. 5(b), open circles correspond to the experiment, and grey corresponds to a simulation that was initialized to include measured vorticity below the shot-noise threshold (grey fuzz in the experimental images). The dashed lines show that the cooling exponent α changes after mergers stop. Both lines correspond to power-law fits of the simulation data. Time t is normalized to the rotation period of the vortex crystal in the simulation where the shot-noise is removed, $\tau_{rot} = 0.23$ ms.

additional merger at $t/\tau_{rot} \approx 100$ or from an interaction with the low-vorticity (below the shot-noise threshold) background that was added to the exterior flow.

We end this section with a brief word on the uncertainty in the number of intense vortices M and in the measure of chaotic vortex motion δv_{rms}. To calculate M and δv_{rms} we used an automated vortex survey.[18] This survey has adjustable parameters ζ_{min} and d_{min} that are used to identify intense vortices in a turbulent flow. Recall that a vortex is defined to be a connected patch of vorticity for which $\zeta > \zeta_{min}$ and for which the mean diameter $d > d_{min}$. There is good agreement between the experiment and simulation regardless of the common parameters that we choose to analyze them both. However, the exact values of M and δv_{rms} will change with the specific parameter choice. For example, we have calculated $M(t)$ and $\delta v_{rms}(t)$ for Sequence I (Fig. 3) with values of ζ_{min} between 4.5×10^4 and 4.5×10^5 s^{-1} and with values of d_{min} between 2.5×10^{-2} and 7.5×10^{-2} cm. During the initial break-up of the annulus, there were large variations in the number of vortices M due to changes in ζ_{min} and d_{min} ($\delta M/M \sim 1$). However, the uncertainty in M dropped to $\sim 10\%$ after 1 rotation period and to 0% after the last merger. Before the last merger, the uncertainty in δv_{rms} was $\sim 20\%$ on average. After the last merger, the uncertainty in δv_{rms} dropped to less than 5%.

IV. DISCRETIZATION EFFECTS AND VISCOSITY

A magnetized electron column and a VIC simulation both consist of a finite number of point-vortices, N. (The electron column consists of N lines of charge, each line charge corresponds to an electron trajectory averaged over the fast axial motion.) The 2D Euler equations govern the ensemble averaged vorticity distribution of a point-vortex gas only in the lowest order mean-field approximation, which neglects fluctuations due to finite N. These fluctuations are thought to cause the slow dissipation of vortex crystals that is observed in experiments with magnetized electron columns. An example of this dissipation process is shown in
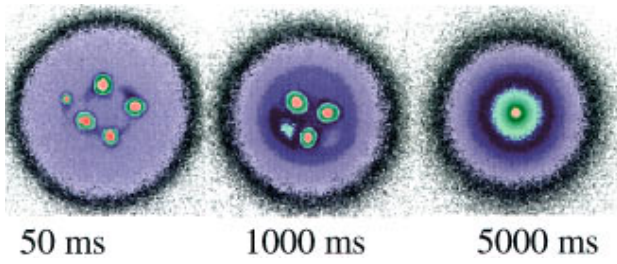
FIG. 7. Dissipation of a metastable vortex crystal in an experiment. This dissipation is believed to be a finite N effect and approximately conserves H/Γ_{tot}^2 and $P_\theta/\Gamma_{\text{tot}}$. The color map is the same as in Fig. 3.

Fig. 7. Here, the decay occurs between 500 and 1000 rotation periods. The dissipation time scale is much greater than the time required for the system to reach a metastable vortex crystal equilibrium (~ 10–100 rotations), but this fact alone does not eliminate the possibility that fluctuations due to finite N drive vortex cooling.

A statistical treatment of finite N effects leads to a collision term on the right-hand side of the continuity Eqs. 1(a) or 2(a). Unlike the constant viscosity ν of Navier–Stokes flow that leads to a simple diffusion of vorticity along streamlines, $\partial\zeta/\partial t + \mathbf{v}\cdot\nabla\zeta = \nu\nabla^2\zeta$, the collision term of a point-vortex gas conserves H and P_θ. The correct form for the collision term of a point-vortex gas is still unresolved and is a topic of current research. For the case of axisymmetric ζ, a Klimontovich approach has been used to derive an explicit result.[16] A more general equation for the collision term has yet to be published. However, as N decreases the collision term should have an increasing effect on the evolution of ζ.

We examined the importance of finite N effects on the formation of vortex crystals by changing the number of point-vortices in a simulation [Fig. 3(b)] from 8×10^5 to 4×10^5 to 1×10^5. For $N=4\times10^5$ and 1×10^5 an additional small vortex appeared in the final crystal, but the total circulation of the intense macroscopic vortices, $\Sigma_{i=1}^M\Gamma_i$, remained the same within 5%. Furthermore, the cooling curves for $N=4\times10^5$ and 1×10^5 fall within the scatter of the cooling curve for $N=8\times10^5$ [Fig. 4(b)]. This result suggests that the finite number of point-vortices is not important to the observed vortex cooling. This argument is strengthened by the fact that the experiment (Sequence I) has $\sim 10^8$ particles and cools at the same rate as the simulations.

We have also increased the grid-point spacing in the simulation by factors of 2 and 4, keeping N fixed at 8×10^5 particles. Once again, only subtle changes were observed. When the grid-point spacing was doubled, 2 additional vortices appeared in the vortex crystal. When the grid-point spacing was increased by a factor of 4, the two small vortices dissappeared. In both cases, the cooling curves overlapped the original, within the scatter of the data.

While on the topic of nonideal effects, it is also of interest to estimate the minimum level of viscosity in the Navier–Stokes equations that is required to prevent the formation of a vortex crystal. Specifically consider Sequence I, where a vortex crystal forms from an unstable annulus (Fig. 3). In Sequence I, the final merger occurs at $T\approx6$ ms (5.6 rotations). After mergers stop, the spacing L between vortex centers is ~ 1 cm and the average vortex radius ρ satisfies the condition $\rho < L/3.2$, which is required to prevent pairwise mergers.[21]

Now consider a flow with the same annular initial condition but with kinematic viscosity ν. Over time, viscosity will expand each vortex such that $\rho \sim \sqrt{4\nu t}$. Define the critical viscosity ν_c by the equation $\nu_c \equiv (L/3.2)^2(1/4T)$. If $\nu \gtrsim \nu_c$, the expanded vortices at time T will not be stable against mergers in the vortex crystal configuration. In other words, if $\nu \gtrsim \nu_c$, viscosity should prevent the formation of a vortex crystal. For Sequence I, ν_c is approximately 4 cm^2/s.

It is possible to model Navier–Stokes viscosity in a VIC simulation by adding a Gaussian random walk to the fluid drift of each point-vortex.[11] Figures 8(a) and 8(b) show the evolution of the annulus in Sequence I with $\nu = 0.127$ cm^2/s and $\nu = 1.27$ cm^2/s, respectively. Once again, the simulations use 8×10^5 point-vortices and a 513×513 square grid. In Fig. 8(a), the vorticity distribution evolves into a pattern that resembles a vortex crystal. The estimated time for viscosity to generate a merger instability in this pattern is ~ 190 ms, which is well beyond the simulation's run time. In Fig. 8(b), there appears to be no intermediate time scale during which the flow can be described as a vortex crystal. This result more or less agrees with our expectation that a vortex crystal should not form if $\nu \gtrsim \nu_c$.

To summarize our observation in dimensionless terms, we define a Reynolds number R by the equation $R \equiv \Gamma_{\text{tot}}/\nu$. In Fig. 8(a) $R = 8.7\times10^5$, and in Fig. 8(b) $R = 8.7\times10^4$. It is apparent from Fig. 8 that vortex crystals will form in Sequence I only if $R \gg 10^5$.

V. IDEAL FLUID MECHANISM FOR VORTEX COOLING

In this section, we address the question of how 2D Euler flow can bring a system that consists of intense self-trapped vortices and a diffuse background of small scale vorticity filaments to a vortex crystal equilibrium. This relaxation is described by the cooling curve $\delta v_{\text{rms}}(t)$, where δv_{rms} is the root-mean-square velocity fluctuation of the intense vortices. As the flow relaxes to a vortex crystal equilibrium, the chaotic advection of the intense vortices cools and δv_{rms} tends to zero. In Sequence I, vortex cooling continues indefinitely after mergers stop (Fig. 4), indicating that there exists a cooling mechanism that is independent of merger events. Such cooling would not occur if the intense vortices were simply advecting in their mutual fields like an isolated Hamiltonian system of point-vortices. However, the vortices are not isolated in that they can interact with the background.

Recall from the introduction that the observed vortex crystals are in excellent agreement with states that maximize disorder (fluid entropy) in the background.[12] According to the regional maximum fluid entropy theory, vortex cooling is caused by the ergodic mixing of the diffuse background by the intense vortices. If the vortices are unable to mix the background, then no vortex cooling should occur, as verified by the following numerical results.

First consider Sequence I [Fig. 3(b)] at 14 rotation periods, after which the number of intense vortices M and the
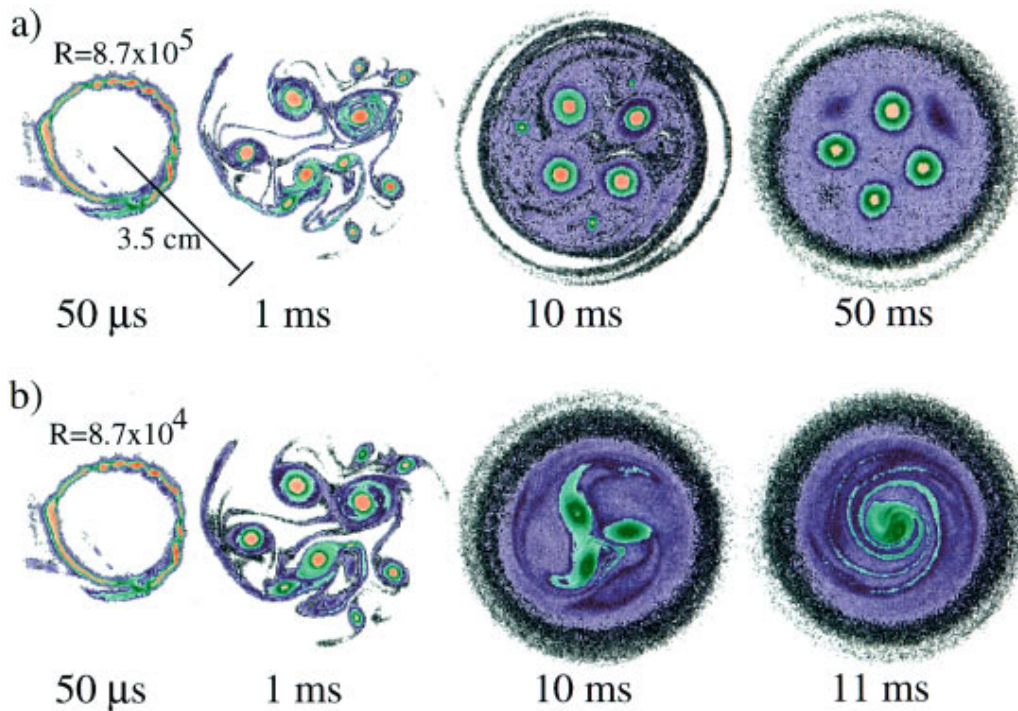
FIG. 8. The effect of viscosity in the Navier–Stokes equations. (a) The evolution of an unstable annulus to a vortex crystal with viscosity $\nu=0.127$ cm^2/s added to the simulation. (b) When $\nu=1.27$ cm^2/s, the viscosity is sufficiently high to prevent formation of a vortex crystal. The color map is the same as in Fig. 3, and the evolution is shown in a reference frame that rotates with frequency 5.872×10^3 rad/s. The Reynolds number R is defined in the text.

total circulation of the intense vortices $\Sigma_{i=1}^M \Gamma_i$ remain fixed. Suppose that all vorticity below $\zeta\approx10^4$ s^{-1} is artificially removed from the simulation at this time, leaving only the intense vortices. Evolving this artificial system forward, we observe no cooling of the vortex motion. This result is shown in Fig. 9 and indicates that vortex cooling is not caused by internal motions within the vortices.

Figure 10 offers a more detailed description of how the cooling exponent α varies with the ratio of the background circulation Γ_b to the total circulation Γ_{tot} (the difference between Γ_{tot} and Γ_b is $\Sigma_{i=1}^M \Gamma_i$, the total circulation in the intense vortices). To obtain these data, the original background vorticity was multiplied by constants ranging from 0 to 3. Circles correspond to Sequence I (starting at 14 rota-

tions) and squares correspond to Sequence II (starting at 172 rotations). In both sets of simulations, the number of intense vortices M remained fixed, with the exception of the data point to the far right, in which a small vortex was sheared apart toward the end of the simulation. As the background vorticity level increases from zero, vortex cooling increases and we observe growth in α. As Γ_b/Γ_{tot} continues to increase, α reaches a maximum value and then begins to fall.

A rise and fall of α as Γ_b/Γ_{tot} increases from 0 to 1 is consistent with our view that vortex cooling (in the absence of mergers) requires the turbulent mixing of an inhomogeneous background by the intense vortices. When there is no
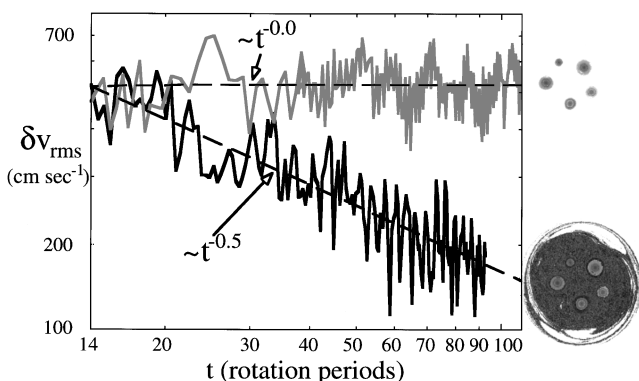

FIG. 9. Cooling curves for vortex crystal with (black) and without (grey) background vorticity. Time t is normalized to the rotation period of the vortex crystal with background vorticity, $\tau_{rot}=1.07$ ms.
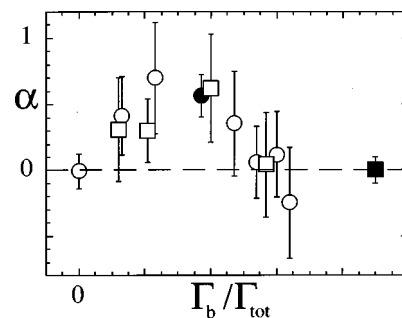

FIG. 10. Cooling exponent α vs Γ_b/Γ_{tot}. Circles correspond to Sequence I [Fig. 3(b)] starting at $t\approx15$ ms (14 rotation periods), and squares correspond to Sequence II [Fig. 5(b)] starting at $t\approx40$ ms (172 rotation periods). The dark symbols mark the cooling exponents for the original simulated flows. To obtain the remaining data, the original background vorticity ($\zeta\leq1\times10^4$ s^{-1} in Sequence I; $\zeta\leq6.8\times10^4$ s^{-1} in Sequence II) was multiplied by constants ranging from 0 to 3.

background, there is no vortex cooling. When $\Gamma_b/\Gamma_{\text{tot}}$ is close to 1, the velocity field is dominated by the contribution from the background vorticity. Presumably, the cooling rate becomes small in this limit because the vortices essentially become passive test particles and lose their capacity to mix the background.

VI. CONCLUSION

The conventional picture of freely relaxing 2D turbulence (with a single sign of vorticity) involves the chaotic advection of intense vortices punctuated by occasional mergers until only a single vortex remains. In experiments with magnetized electron columns, we have seen that mergers can stop due to the spontaneous formation of a vortex crystal. In this paper, we have argued that the observed vortex crystals can be explained without incorporating physics beyond 2D Euler theory [Eq. (2)], despite small differences between a magnetized electron column and an ideal 2D fluid. Our argument was based on a comparison of two experiments to the results of a VIC simulation that numerically integrates the 2D Euler equations. We found good quantitative agreement in the evolution of the number of intense vortices M and in the cooling of their chaotic advection, described by $\delta v_{\text{rms}}(t)$.

Even so, there were some issues to address. A magnetized electron column and a VIC simulation both consist of a finite number of point-vortices N. The 2D Euler equations govern the ensemble averaged vorticity distribution of a point-vortex gas only in the lowest order mean field approximation, which neglects fluctuations due to finite N. A statistical treatment of these fluctuations leads to a collision term on the right-hand side of the continuity equation 2(a), which goes to zero as N goes to infinity and the fluctuations become negligible.[16] There was concern that the collision term due to finite N was responsible for vortex cooling. However, the cooling curve $\delta v_{\text{rms}}(t)$ did not change in Sequence I (Fig. 3) when N was decreased from 8×10^5 to 4×10^5 to 1×10^5 [Fig. 4(b)]. Moreover, the simulation curves fell within the scatter of the cooling curve for the experiment, which had $N\sim10^8$ point-vortices. These results strongly suggest that finite N effects are not important to the formation of vortex crystals.

Another question concerned viscosity in the Navier–Stokes equations. In Sec. IV, we showed that a small level of viscosity can destroy the process of vortex crystal formation entirely (Fig. 8). Specifically, we found that Sequence I requires a Reynolds number $R\equiv\Gamma_{\text{tot}}/\nu$ much greater than 10^5 to produce a vortex crystal. For $R\lesssim10^5$, viscosity expands the vortices sufficiently fast so that they merge before they have time to settle into a vortex crystal geometry.

We have also discussed a mechanism for vortex cooling that is consistent with inviscid incompressible 2D fluid dynamics [Eq. (2)]. In a recent paper,[12] Jin and Dubin showed that vortex crystals are well described as states that maximize an entropy functional of the background vorticity distribution, subject to the constraints of 2D Euler flow. This result suggests that the system is driven to a vortex crystal

equilibrium through a process that requires the ergodic mixing of the background vorticity.

When the background circulation is much less than the combined circulation of the intense vortices (but not zero), it is reasonable that the vortices can perform the required mixing. On the other hand, when the background circulation dominates, the vortices become less effective mixers. Therefore, if vortex cooling is driven by the turbulent mixing of the background by the intense vortices, the cooling rate should first rise and then fall as Γ_b increases from zero. Our simulation results are consistent with this picture (Fig. 10). When the background was removed, there was no vortex cooling and the intense vortices remained out of equilibrium. Only when the intense vortices were immersed in a low level of background vorticity did they cool toward a pattern in uniform rotation. As $\Gamma_b/\Gamma_{\text{tot}}$ was adjusted closer to 1, the rate of vortex cooling dropped below the accuracy of our measurements.

Finally, we note that the vorticity distributions in magnetized electron columns have two distinct features that may contribute to the arrest of vortex mergers and to the formation of vortex crystals. First, they have a single sign of (positive) vorticity. The effect on vortex crystal formation of adding negative vorticity to the flow is a subject of current research. Second, the background vorticity has a sharp edge where ζ drops rapidly to zero. The interaction between the intense vortices and surface-waves (Kelvin-waves) at the edge can not be ignored in a general treatment of the dynamics. A detailed study of this nonlinear interaction has recently been carried out and it has been shown to contain a plausible mechanism of vortex cooling at late times.[22]

[1]A. P. Ingersoll, ''Atmospheric dynamics of outer planets,'' Science **248**, 308 (1990); P. S. Marcus, ''Numerical simulations of Jupiter's great red spot,'' Nature (London) **331**, 693 (1988); ''Vortex dynamics in a shearing zonal flow,'' J. Fluid Mech. **215**, 393 (1990)

[2]J. C. McWilliams, ''On the relevance of two-dimensional turbulence to geophysical fluid motions,'' J. Mec. Theor. Appl. **83**, (1983); J. Pedlosky, *Geophysical Fluid Dynamics* (Springer, New York, 1987).

[3]C. F. Driscoll, K. S. Fine, X.-P. Huang, T. B. Mitchell, and B. P. Cluggish, ''Vortices and turbulent relaxation in magnetized electron columns,'' in *Transport, Chaos, and Plasma Physics 2*, edited by S. Benkadda, F. Doveil, and Y. Elskens (World Scientific, Singapore, 1996), pp. 19–29.

[4]M. R. Brown, ''Experimental evidence of rapid relaxation to large-scale structures in turbulent fluids: Selective decay and maximal entropy,'' J. Plasma Phys. **57**, 203 (1996).

[5]D. Lynden-Bell, ''Statistical mechanics of violent relaxation in stellar systems,'' Mon. Not. R. Astron. Soc. **136**, 101 (1967); R. Robert and J. Sommeria, ''Statistical equilibrium states for two-dimensional flows,'' J. Fluid Mech. **229**, 291 (1991); J. Miller, P. B. Weichman, and M. C. Cross, ''Statistical mechanics, Euler equations, and Jupiter's great red spot,'' Phys. Rev. A **45**, 2328 (1992); A. Thess, J. Sommeria, and B. Jütner, ''Inertial organization of a two-dimensional turbulent vortex street,'' Phys. Fluids **6**, 2417 (1994); L. Onsager, ''Statistical hydrodynamics,'' Nuovo Cimento Suppl. **6**, 279 (1949); G. Joyce and D. Montgomery, ''Negative temperature states for the two-dimensional guiding-center plasma,'' J.

Plasma Phys. **10**, 107 (1973); D. L. Book, Shalom Fisher, and B. E. Mc-Donald, ''Steady-state distributions of interacting discrete vortices,'' Phys. Rev. Lett. **34**, 4 (1975); T. S. Lundgren and Y. B. Pointin, ''Statistical mechanics of two-dimensional vortices,'' J. Stat. Phys. **17**, 323 (1977); R. A. Smith and T. M. O'Neil, ''Nonaxisymmetric thermal equilibria of a cylindrically bounded guiding-center plasma or discrete vortex system,'' Phys. Fluids B **2**, 2961 (1990); D. Montgomery, X. Shan, and W. H. Matthaeus, ''Navier–Stokes relaxation to Sinh–Poisson states at finite Reynolds numbers,'' Phys. Fluids A **5**, 2207 (1993).

[6]F. P. Bretherton and D. B. Haidvogel, ''Two-dimensional turbulence above topography,'' J. Fluid Mech. **78**, 129 (1976); W. H. Matthaeus and D. Montgomery, ''Selective decay hypothesis at high mechanical and magnetic Reynolds numbers,'' Ann. NY Acad. Sci. **357**, 203 (1980).

[7]X.-P. Huang and C. F. Driscoll, ''Relaxation of 2D turbulence to a metaequilibrium near the minimum enstrophy state,'' Phys. Rev. Lett. **72**, 2187 (1994).

[8]K. S. Fine, A. C. Cass, W. G. Flynn, and C. F. Driscoll, ''Relaxation of 2D turbulence to vortex crystals,'' Phys. Rev. Lett. **75**, 3277 (1995).

[9]L. J. Campbell and R. M. Ziff, ''Vortex patterns and energies in a rotating superfluid,'' Phys. Rev. B **20**, 1886 (1979).

[10]A. Leonard, ''Vortex methods for flow simulations,'' J. Comput. Phys. **37**, 288 (1980); C. K. Birdsall and A. B. Langdon, *Plasma Physics Via Computer Simulation* (Adam Hilger, New York, 1991).

[11]A. J. Chorin, ''Numerical study of slightly viscous flow,'' J. Fluid Mech. **57**, 785 (1973).

[12]D. Z. Jin and D. H. E. Dubin, ''Regional maximum entropy theory for vortex crystal formation,'' Phys. Rev. Lett. **80**, 4434 (1998).

[13]R. J. Briggs, J. D. Daugherty, and R. H. Levy, ''Role of Landau damping in crossed-field electron beams and inviscid shear flow,'' Phys. Fluids **13**, 421 (1970); C. F. Driscoll and K. S. Fine, ''Experiments in vortex dynamics in pure electron plasmas,'' Phys. Fluids B **2**, 1359 (1990); R. C. Davidson, *Physics of Non-Neutral Plasmas* (Addison–Wesley, Reading, 1990), pp. 289–311.

[14]R. A. Smith, ''Effects of electrostatic confinement fields and finite gyroradius on an instability of hollow electron columns,'' Phys. Fluids B **4**, 287 (1992); C. F. Driscoll, ''Observation of an unstable $l=1$ diocotron mode on a hollow electron column,'' Phys. Rev. Lett. **64**, 645 (1990).

[15]A. J. Peurrung and J. Fajans, ''A limitation on the analogy between pure electron plasmas and two-dimensional inviscid fluids,'' Phys. Fluids B **5**, 4295 (1993).

[16]D. H. E. Dubin and T. M. O'Neil, ''Two-dimensional guiding-center transport of a pure electron plasma,'' Phys. Rev. Lett. **60**, 1286 (1988); ''Two-dimensional bounce-averaged collisional particle transport in a single species non-neutral plasma,'' Phys. Plasmas **5**, 1305 (1998).

[17]Many papers on the statistical mechanics of 2D turbulence discuss the effect of coarse-graining on the integral invariants of 2D Euler flow. See, for example, J. Miller, ''Statistical mechanics of Euler equations in two dimensions,'' Phys. Rev. Lett. **65**, 2137 (1990).

[18]J. C. McWilliams, ''The vortices of two-dimensional turbulence,'' J. Fluid Mech. **219**, 361 (1990).

[19]G. F. Carnevale, J. C. McWilliams, Y. Pomeau, J. B. Weiss, and W. R. Wang, ''Evolution of vortex statistics in two-dimensional turbulence,'' Phys. Rev. Lett. **66**, 2735 (1991).

[20]S. Chandrasekar, ''Stochastic problems in physics and astronomy,'' Rev. Mod. Phys. **15**, 1 (1943).

[21]K. S. Fine, C. F. Driscoll, J. H. Malmberg, and T. B. Mitchell, ''Measurements of symmetric vortex merger,'' Phys. Rev. Lett. **67**, 588 (1991).

[22]D. Z. Jin and D. H. E. Dubin, ''Dynamics of vortex crystals,'' Bull. Am. Phys. Soc. **42**, 2056 (1997).